The effect of the tip vortex on the flow around a circular cylinder

Cesar Monzu Freire, cesar.freire@usp.br
Ivan Korkischko, ivan.korkischko@usp.br
Julio R. Meneghini, jmeneg@usp.br
NDF, Department of Mechanical Engineering, POLI, University of São Paulo, CEP 05508-900, São Paulo, SP, Brazil

Abstract. *: It is known that the end conditions can affect the flow around bluff and slender bodies. A lot of effort has been done about the so-called infinity structures, which have high values of aspect ratio and are usually assumed to cause a two-dimensional flow. Some of these studies try to eliminate the tip vortex by employing end-plates which force the flow to be parallel at the end of the body. There is another line of research that focus on the flow around bodies with small aspect ratio. The focus of this work is to study the influence of the tip vortex on the flow around circular, smooth and fixed cylinders in order to analyze under what circumstances the effect of the tip vortex can be ignored and when the tip vortex affects significantly the flow. Stereoscopic particle image velocimetry has been employed to measure the flow field and a technique of volumetric reconstruction has also been used to obtain the three-dimensional mean flow. Besides flow visualization, the drag force has been measured in order to study the effects of tip vortex on the hydrodynamic force.*

Keywords: *tip vortex, vortex-shedding, flow past cylinder, stereoscopic particle image velocimetry*

1. INTRODUCTION

The flow around bluff bodies is a very common situation in nature and in engineering applications. Depending on the fluid velocity, its viscosity, the body geometry, among several other characteristics, the flow can present different behaviors from just passing around the body in a smooth and almost gentle way until causing intense and oscillatory forces that can induce the body to vibrate and even leading it to failure. One of these interactions occurs when the vortex shedding around the body create an oscillatory pressure field that can provoke the cylinder to vibrate in what is called vortex-induced vibration (VIV). This phenomenon affects many different areas in engineering, such as building, bridges, offshore structures to mention just a few.

A lot of research has been done to reveal the main features of different kinds of flow. One of the most studied cases is the flow around circular cylinders that can be justified by two main reasons. First, this is one of the most simple geometries that can be studied. Second, despite the simple geometry, the flow around cylinder presents different fluid dynamic phenomena which make the problem very rich and interesting.

Thinking about smooth and rigid circular cylinders, there are only two characteristics lengths to be taken into account: the cylinder diameter D and immersed length L. As a combination of these two lengths, the aspect ratio (AR) can be defined as $AR = L/D$. It is expected that for long cylinders, with very high aspect ratios, the main features of the flow are different when compared to the flow around short cylinders with low aspect ratios. This difference is caused by the end effects that are strongly three-dimensional.

In engineering, both situations, high and low AR, can be found and a good understanding of both is primordial. Some buildings can be considered cylinders with low aspect ratios while chimneys have larger AR. In the offshore industry, for example, both kinds of flows can be found. For the riser tubes that brings the oil from the sea bed to the surface the flow is considered to be very close to the two-dimensional case because the aspect ratio is so high that three-dimensional effects can be, in first order, ignored. In the other hand, the flow around some platforms, like the monocolumn type, are strongly affected by the three-dimensional effects of the flow. Because of the importance of the three-dimensional effects there is a distinction between the VIV and VIM (vortex-induced motions) where the first is used for long cylinders like riser tubes and mooring lines and the second is used for structures with low aspect ratios as monocolumn platforms. The three-dimensional flow features cited above are not related to the three-dimensional instabilities that occur in the flow past a cylinder, but the ones caused by the geometric effects.

Because of its engineering significance, and consequent economic appeal, the end effects have been intensively studied. Most of these studies have focused on rigid fixed cylinders immersed in a current flow with one free end. This situation is very close to several practical applications where a short cylinder is mounted over a surface. It was found that depending on AR the classical vortex shedding pattern, known as the von Kármán street, is suppressed and other vortex patterns are formed. More about the flow around fixed cylinders with low aspect ratios can be found in Summer *et al.* (2004),Fröhlich and Rodi (2004) and Pattenden *et al.* (2005).

The effects of the end conditions in VIV were recently studied by Morse *et al.* (2008). Motivated by the diferences found in free and forced oscillations in VIV, the authors studied how the end condition, controlled by the use of end-plates, can affect the amplitude response. Three conditions were tested by the authors: end plate attached to the bottom of a vertical and rigid cylinder, end plate not attached to the cylinder but mounted just below it with a small gap between them

and the last condition where no end plate was used. They concluded that the case with attached end plate and the case with no attached end plate presented the same response if the gap between the end plate and the cylinder was higher then 0.15 times the cylinder diameter. For gaps higher then this threshold value the response observed was very close to the one obtained for the case without end-plate. They also founded that the setup without end-plates had a higher amplitude response when compared to classical amplitude response obtained with end-plates. Besides that the abrupt upper-lower branch transition was suppressed to a smooth decrease of amplitude in the case without end-plate.

All these results and differences caused by the end conditions motivate the present work. In this paper a stereoscopic particle image velocimetry (SPIV) is used to measure the flow field in several plains close to the cylinder extremity and a reconstruction technique is used to remount the three-dimensional (volumetric) wake flow. This technique has been employed by Korkischko *et al.* (2010) to visualize the three-dimensional wake formed by the flow past a straked cylinder. Along with the flow visualization, drag measurements were conducted in order to verify how much the end conditions could change the hydrodynamic forces acting on the cylinder.

2. Experimental procedure

The experiments were conducted in the recirculating water channel facility at the Fluid & Dynamic Research Group (NDF) at the University of São Paulo (USP). The recirculating water channel facility has a $0.7 \times 0.8 \times 7.5m$ test section with free surface, can operate with very low turbulence level ($Tu < 2\%$) up to flow velocities $0.7m/s$ and has the walls and the floor made of glass that allows a complete flow visualization. A rigid and smooth acrylic cylinder with $32mm$ of external diameter was used as model.

Two different experimental approaches were used in this paper. To visualize the flow a SPIV technique was employed in 25 different planes close to the cylinder extremity. The same flow velocity was used in all visualizations keeping a constant $Re = 5000$. For the drag measurements a load cell capable of measuring force and torque was attached to the top of the cylinder. Different velocities were tested so a drag coefficient curve was obtained for $2000 < Re < 8000$. More details about each experimental approach are presented in the next subsections.

2.1 Flow visualization

For the flow visualization a LaVision SPIV Quantel (Brilliant Twins) double-cavity pulsed Nd:YAG laser with 532nm wavelength was used to illuminated a plane in the flow and two Imager Pro X 2 Megapixel cameras equipped with Nikon (AF Nikkor f/1.4D) 50mm focal length lenses were used to record the illuminated region. The visualized plane is horizontal and the acquisition area is recorded by the cameras mounted below the water channel. As can be seen in figure 1, the cameras were mounted in angle with the vertical in order to allow the stereoscopic acquisition. If the cameras had been mounted in the vertical position they could only measure the velocity components in the acquisition plane. More about PIV can be found in Adrian (1991) and about SPIV in Prasad (2000).

The cylinder was fixed vertically by the assembly shown in figure 1(b) that is capable of easy and accurate vertical movement of the cylinder and can resist the hydrodynamic forces and moments acting on the cylinder. The SPIV acquisition system was calibrated for a specific height of the water column and all visualized planes were measured at the same plane. In order to study different planes with respect to the end of the cylinder it had to be moved vertically. Each acquisition consisted on recording 345 pictures taken with $14.8Hz$, which is the maximum laser frequency of operation, giving close to 23 seconds of acquisition. With these 345 instantaneous velocity fields a mean velocity field and a RMS velocity field were calculated. To mount the 345 instantaneous images for each one of the 25 layers into a three-dimensional movie it would be necessary to measure the phase angle between each acquisition but this analysis goes beyond the purposes of the present work.

The visualization area included just a little slice of the cylinder because as the acrylic cylinder would reflect too much light to the cameras it would diminish the visualization quality. Aiming to avoid this problem the cylinder was painted with a rhodamine-based ink that reflects the incident light in a different wavelength that can be filtered by a lens filter.

The SPIV system was calibrated at a distance close to $10D$ above the water channel floor. After the calibration procedure the cameras and the laser cannons were kept at the same configuration. The diference between each case was then obtained by moving the cylinder and the water channel level, always keeping the same immersed length. All 25 planes were obtained revealing the flow along a $10D$ length in the spanwise direction. Both regions above and below the cylinder tip were considered for the visualization. The $10D$ visualized along the spanwise direction consists in $5D$ above the cylinder tip and another $5D$ below it. The total visualized volume is $5D \times 7,5D \times 10D$.

As mentioned before, for each acquisition the water channel height was adjusted to not change the immersed length. Besides changing the water column height, it was necessary to adjust the pump frequency in order to keep the flow velocity constant. The flow velocity chosen for the visualizations were $U = 0.156m/s \pm 0.002$ which gives $Re = 5000 \pm 100$.

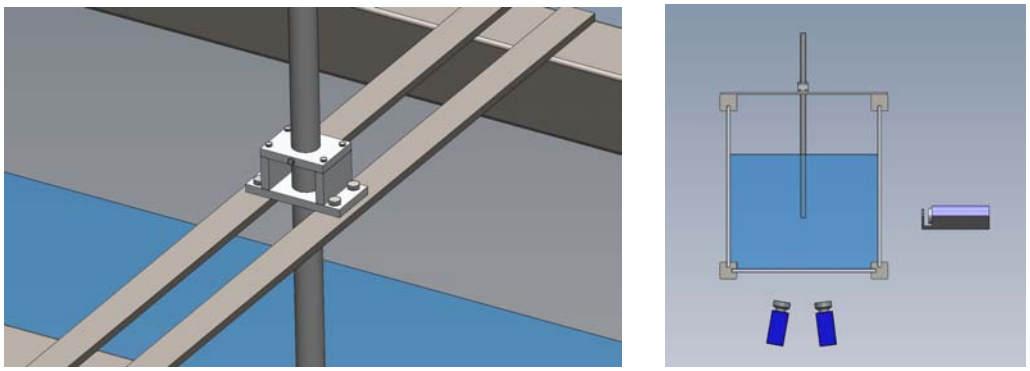

(a) (b)

Figure 1. Front view of the experimental arrangement

2.2 Drag measurement

For the drag measurements, a different experimental arrangement was used. The goal was to verify if the tip vortex affects or not the hydrodynamic forces acting on the cylinder in two different situations. It is expected that a difference in the flow condition cause different forces, but the purpose is to test if this changes are significant enough to be detected.

In the first condition tested, called as lower condition (LC), the cylinder was mounted with its bottom very close to the water channel floor. The cylinder was mounted touching the water channel floor and then lifted just enough to separate them. The gap formed is smaller then $3mm$. This condition is illustrated by the figure 2(a). In the second condition, called as middle condition (MC), the cylinder was lifted to be distant to the floor, allowing the end effects to develop. For MC the gap between cylinder and the floor was close to $340mm$, more then 10 times the cylinder diameter, as can be seen in figure 2(b).

The forces were measured using a ATI mini40 load cell which is able to measure the three components of the force and the three components of the torque. The load cell was mounted out of the water in the top extremity of the cylinder, as shown in figure 2(c).

In order to isolate the end effects, both experiments were conducted with the same aspect ratio ($AR = L_W/D = 10$). The acquisition frequency adopted was $100Hz$ which is well above the maximum vortex shedding frequency on the experiment which is close to $2.5Hz$.

For the first condition (LC) it is expected that the force F and the torque T are related by the equation 1, been L_F the an effective length where the total drag force F is applied. Actually the force acting on the cylinder is caused mostly by the pressure gradient around the cylinder giving a distributed force along the span $f(z)$. If there is no significative three-dimensional effects one may think that the integral along the span would result in a uniform force distribution equivalent to an effective force acting at the middle height of the water column, as indicated in figures 2(c) and 2(d). Following the same idea, it is expected that for the same immersed length L_W, flow velocity U and cylinder diameter D, the effective length would be at least slightly different due to the tip vortex and other end effects. As the force results were not accurate enough to allow this analysis, equation 1 will be assumed to calculate the drag force from the torque signal. It is important to highlight here that the main purpose is to compare two different situations and not to evaluate the hydrodynamics coefficients precisely. As both conditions are treated equally and the results are analyzed by the same methods, a difference in the results would indicate a difference in the responses.

$$T = F\,L_F \tag{1}$$

To verify repeatability and ensure the results accuracy four tests were conducted with the same experimental setup for each condition and inside the same flow velocity range. The only difference between the tests was a slightly difference in the initial flow velocity value or the steps between each point tested. These diferences were imposed in order to verify the response in a more distributed way. The flow velocity was varied in the range $0.03m/s < U < 0.26m/s$, which gives $1000 < Re < 8000$. The maximum flow velocity was selected in order avoid the cylinder vibration. Despite the fact that the cylinder was fixed in a rigid structure, the global system stiffness is not infinity and for some conditions it allowed the cylinder to oscillate, with very little amplitude, but causing a strong force amplification, owing to vortex-induced vibrations, as shown in figure 3. As can be seen in figures 3(a) and 3(b) the vibrations starts for a small change in the flow velocity and cause a significant force amplification.

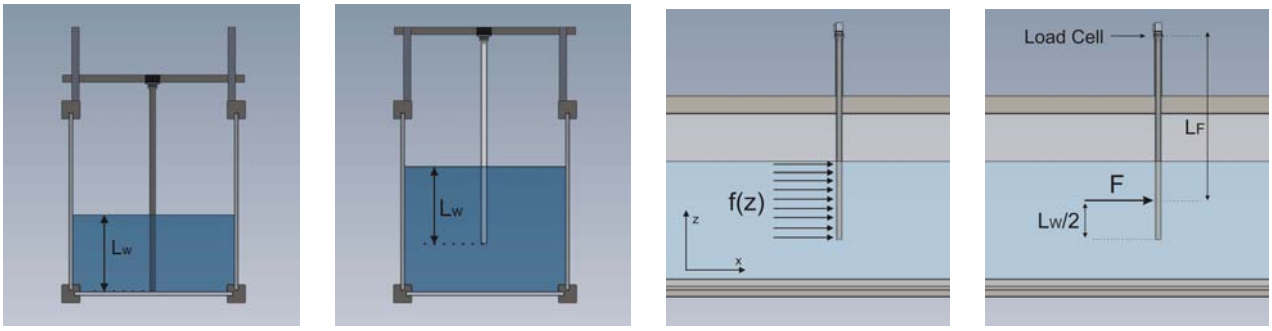

(a) (b) (c) (d)

Figure 2. Experimental arrangement for drag measurements. (a) lower condition (b) middle condition (c) defining L_F (d) representation of the span distributed drag force $f(z)$

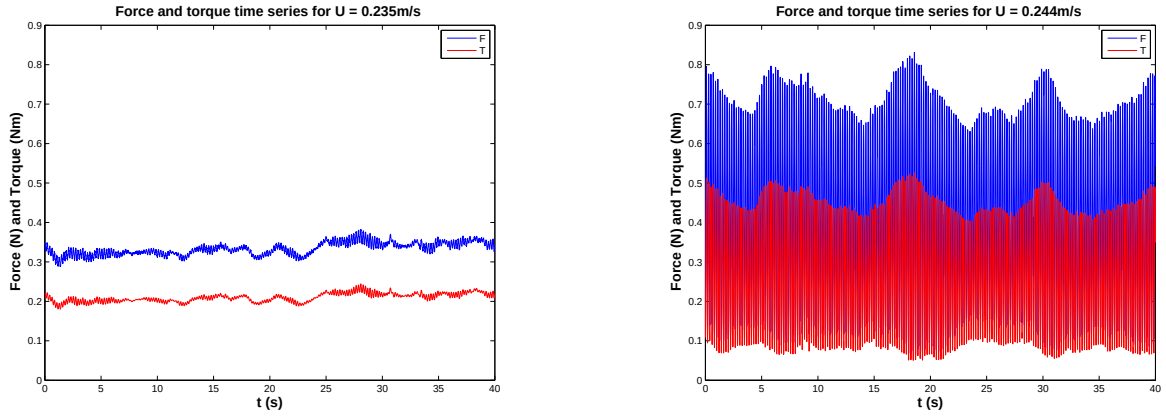

(a) (b)

Figure 3. Experimental results for torque: (a) without uncertainty bars (b) with uncertainty bars

3. Results

3.1 Drag measurement

Figure 4 illustrates the torque acting on the load cell versus the flow velocity. As can be seen in the figure 4(a), there is a remarkable agreement of the results for all eight tests. It is interesting to notice that the data collapse into a parabola which is expected once the fluid forces depends on the U^2.

Figure 4(b) shows the same results with error bar, that is assumed to be standard deviation or the root mean square (RMS) of the recorded signal less its mean value, as indicated in equation 2. N represent the number of acquisitions that is equal to the frequency rate multiplied by the the measurement interval. In all force measurements the acquisition frequency was $100Hz$ and the acquisition time was $120s$ giving $N = 12,000$. The last points shown in figure 4(b), obtained for high flow velocities, present a very high error bar. This is caused by a coupling between the flow and the structure that starts to vibrate due to vortex-induced vibrations. The force and torque time series for the last two points were shown in figure 3. As the focus of this paper is to study the effects of the end vortex for fixed cylinders, these last points will not be taken into account in the next considerations.

$$S_{RMS} = \sigma_S = \sqrt{\sum_{i=1}^{n=N} \frac{(S - S_{mean})^2}{N}} \tag{2}$$

To calculate the drag coefficient from the torque measurements, equation 3, its is necessary, as mentioned before, to adopt an equivalent distance L_F were the drag force is applied. This value was assumed to be the distance between the load cell and the center of the wet length, as defined in figure 2(d), and equals to $811mm$. In equation 3, ρ is the fluid density.

$$C_D = \frac{2\,T}{\rho\,D\,L_W\,U^2\,L_F} \tag{3}$$

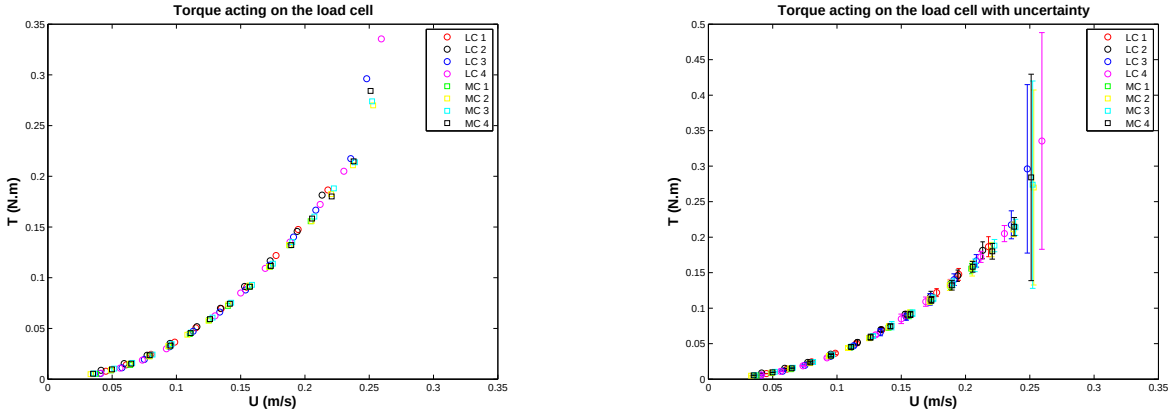

(a) (b)

Figure 4. Experimental results for torque: (a) without uncertainty bars (b) with uncertainty bars

The drag coefficient uncertainty was calculated using equation 4 that considers all uncertainties related to the variables used in equation 3.

$$\sigma_{C_D} = C_D \sqrt{\left(\frac{\sigma_{L_W}}{L_W}\right)^2 + \left(\frac{\sigma_{L_F}}{L_F}\right)^2 + \left(\frac{\sigma_D}{D}\right)^2 + \left(\frac{\sigma_\rho}{\rho}\right)^2 + \left(\frac{\sigma_T}{T}\right)^2 + 2\left(\frac{\sigma_U}{U}\right)^2} \tag{4}$$

The geometric uncertainties and σ_ρ are very small and do not contribute significantly to σ_{C_D}. The most importante sources of uncertainty are σ_U and σ_T. Both are consider to be the standard deviation of the acquired signal. The mean σ_{C_D} obtained for all testes is close to $\sigma_{C_D} = 0.05$.

$$C_{D_{LC}} = 0.92 \pm 0.05$$
$$C_{D_{MC}} = 0.89 \pm 0.05$$

Calculating the mean value of C_D inside $2000 < Re < 7800$ the drag coefficients obtained are $C_{D_{LC}} = 0.92$ and $C_{D_{MC}} = 0.89$. This small diference can be noticed in figure 5(a) where the circles are above the square dots. Despite this fact, considering the mean uncertainty of the measurement, one can not attest that the forces have changed or not, as depicted by figure 5(b) where all results are at the same zone.

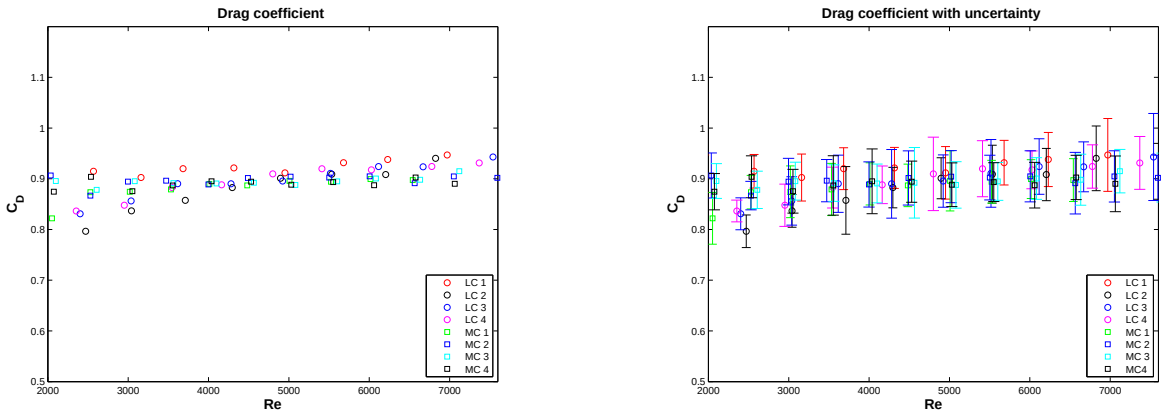

(a) (b)

Figure 5. Drag coefficient: (a) without uncertainty bars (b) with uncertainty bars

3.2 Flow visualization

In this section the flow visualization around the immersed cylinder tip is presented. Owing to the difficulty to illustrate three-dimensional flow features with pictures, sections were used to represent the main flow characteristics. Figure 6 defines the three different planes used to represent the flow, being a side view, a front view and a top view. In the side

view figures the black strip represents the cylinder. The same orientation used previously is applied in this section. In all figures the velocity fields were non-dimensionalised by the mean in-line velocity $U = 0.156m/s$. The flow is from the left to the right.

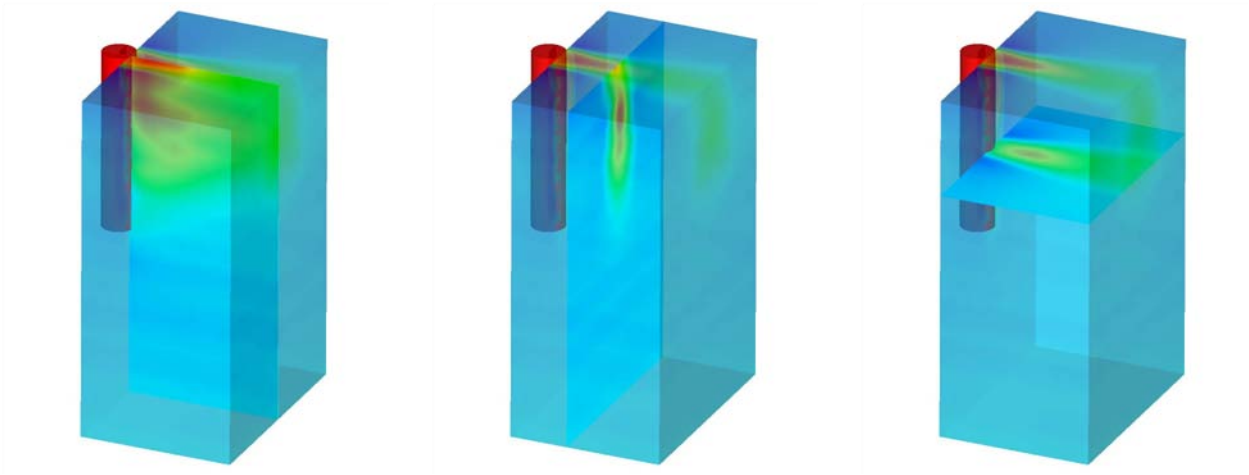

(a) (b) (c)

Figure 6. Defining visualization planes (a) side view (b) front view (c) top view. The flow is from the left to the right.

As mentioned in the experimental procedure, 345 images were obtained for each height. With all the images a mean and a RMS flow field were calculated. The idea of the RMS flow field is to search for areas where there the flow change along the time. Looking for those areas the U_{RMS} velocity, defined by the equation 5, was used. This parameter measures the fluctuation of all the three components of the velocity, so if there is any disturbance on the flow it would be indicated by $U_{RMS} > 0$. Figure 7(a) depicts the iso-surface of the non-dimensionalised RMS velocity U_{RMS}/U. As it is expected for the flow around circular cylinders with Reynolds number higher than 46, where the vortex-shedding starts, the region behind the cylinder will present a vortex street. Owing to that fact, the RMS field is expected to be nonzero because the velocity chances as a function of the time inside that region. As can be seen in figure 7(a), close to the cylinder extremity there is no vortex-shedding. The disturbed region grows from the tip and in a small distance, close to $1.3D$, reaches the developed vortex street. The side view shown in figure 7(c) illustrates that property.

$$U_{RMS} = \sqrt{Ux_{RMS}^2 + Uy_{RMS}^2 + Uz_{RMS}^2} \tag{5}$$

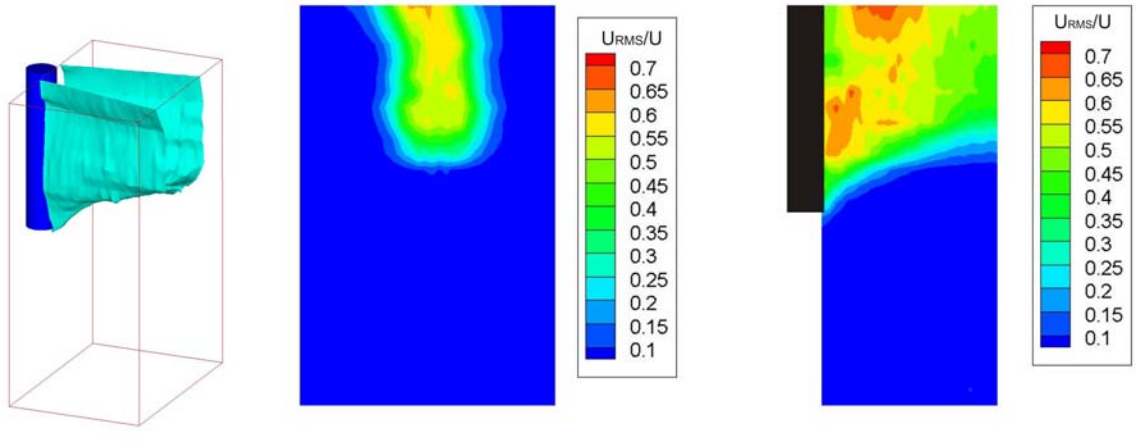

(a) (b) (c)

Figure 7. U_{RMS}/U (a) 3D iso-surface (b) front view (c) side view. The flow is from the left to the right.

The mean flow velocities, shown in figure 8, allow the understanding of why the region close to the cylinder tip does not develop a vortex street. As can be seen in figure 8(a), the first key point that should be highlighted is that below the cylinder the flow is barely affected by its presence while in the recirculation region formed behind the cylinder the velocity is strongly reduced. The in-line flow velocity gradient can also be seen in figure 8(c) which evidences that just the region behind the cylinder has its velocity reduced while in the rest of the flow the velocity is uniform.

Owing to that gradient of velocity the flow behind the cylinder has its vertical component negative as pointed out by the current lines in figures 8(a) and 8(b). Figure 8(d) illustrates the cross-flow component of the velocity behind the cylinder. This picture is easy to understand because it shows that flow the fills in the empty space once occupied by the cylinder. The flow coming from the right side of the cylinder goes to the left $Uy/U < 0$ and the flows coming from the left side goes to the right $Uy/U > 0$.

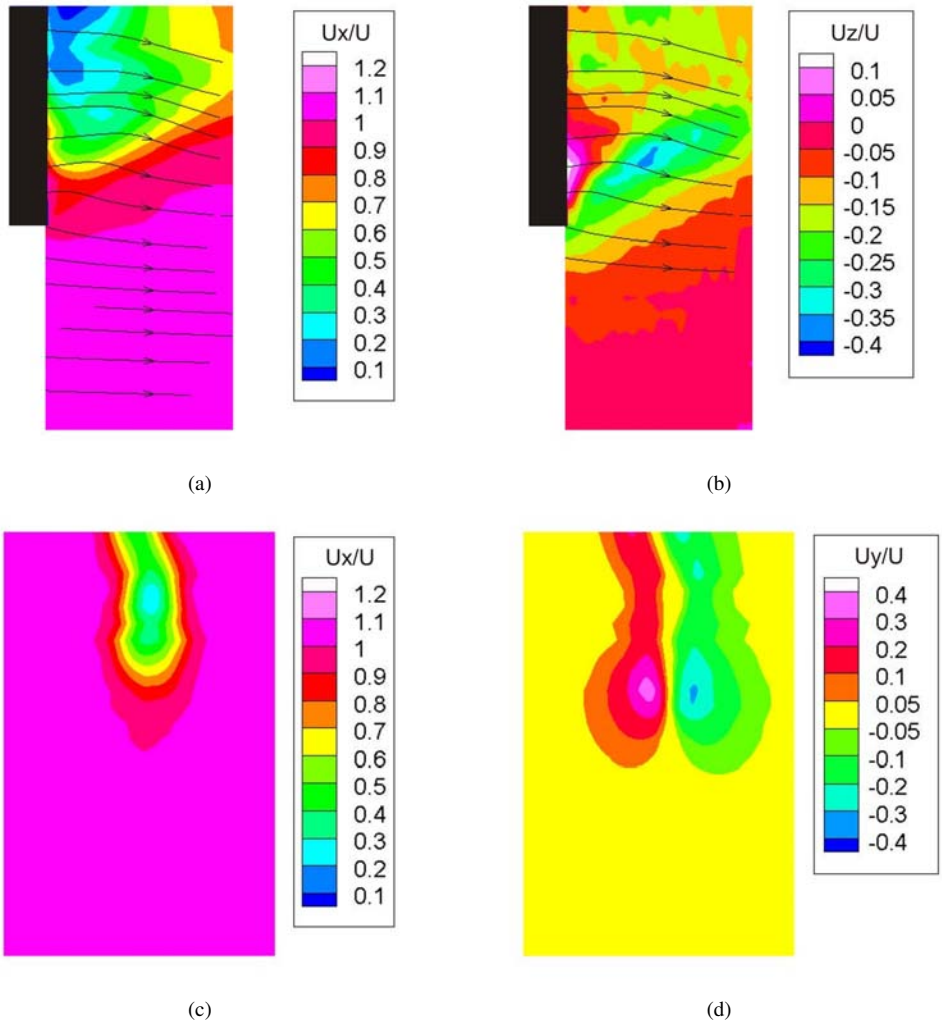

Figure 8. Side view: (a) in-line velocity U_x/U (b) vertical velocity U_z/U. The flow is from the left to the right. Front view: (c) in-line velocity U_x/U (d) cross-flow velocity U_y/U.

4. Conclusions

Two different approaches were employed in this work in the interest to study the topology and effects of the tip vortex. Drag measurements were conducted to verify if the end conditions could cause a measurable change in the hydrodynamics forces. Two conditions were tested: with and without end effects. To avoid the end effects the cylinder was mounted so its end was very close to the water channel floor. The condition with end effects was tested with a big gap between the cylinder tip and the floor. The load cell used in the experiment provided accurate torque measurements that collapsed remarkably well for all tests. Considering the experimental uncertainties no difference between LC and MC could be detected.

For the visualization part, it was verified that near the cylinder tip there is no vortex-shedding and no vortex street develops. The flow passing below the cylinder is barely affected by its presence and the flow that passes around the cylinder gain a negative vertical velocity. The downwash flow suppress the vortex-shedding at the cylinder tip.

Despite the influence of the end effects on the flow around a finite circular cylinder and a diminishing of a region under the vortex shedding, the likely change in the hydrodynamic forces was so little that it could not be measured experimentally.

This is the first part of an ongoing research about the end effects in VIV and fixed cylinders. Future works will consider

the application of end plates and the study of the end effects for lower aspect ratios where the authors expect to find the end effects more relevant to the hydrodynamic forces acting on the cylinder.

5. Acknowledgements

The authors would like to acknowledge the financial support provided by Fapesp, CNPq, FINEP and Petrobras.

6. References

Adrian, R.J., 1991. "Particle-imaging techniques for experimental fluid mechanics". *Annual Review of Fluid Mechanics*, Vol. 23, pp. 261–304.

Fröhlich, J. and Rodi, W., 2004. "Les of the flow around a circular cylinder of finite height". *International Journal of Heat and Fluid Flow*, Vol. 25, pp. 537–548.

Korkischko, I., Freire, C.M., Meneghini, J.R. and Franciss, R., 2010. "Vortex-induced vibrations and wake structures of isolated plain and straked cylinders mounted on a 2dof elastic base". In *Proceedings of the 29th International Conference on Ocean, Offshore and Artic Engineering, OMAE 2010.*

Morse, T.L., Govardhan, R.N. and Williamson, C.H.K., 2008. "The effect of end conditions on the vortex-induced vibration of cylinders". *Journal of Fluid and Structures*, Vol. 24, pp. 1227–1239.

Pattenden, R.J., Turnock, S.R. and Zhang, X., 2005. "Measurements of the flow over a low-aspect-ratio cylinder mounted on a groud plane". *Experiments in Fluids*, Vol. 39, pp. 10–21.

Prasad, A.K., 2000. "Stereoscopic particle image velocimetry". *Experiments in Fluids*, Vol. 29, pp. 103–116.

Summer, D., Heseltine, J.L. and Dansereau, O., 2004. "Wake structure of a finite circular cylinder of small aspect ratio". *Experiments in Fluids*, Vol. 37, pp. 720–730.

7. Responsibility notice

The authors are the only responsible for the printed material included in this paper.